

Evaluation of oxides formed at high temperature in Zr-2.5Nb pressure tubing

N.A.P.Kiran Kumar¹, J.A.Szpunar¹

¹ University of Saskatchewan, Saskatchewan, Canada
(Email: kiraniitkgp@yahoo.com)

Abstract

The oxidation behavior of Zr-2.5Nb pressure tube samples has been studied at four different temperatures, i.e., 400°, 600°, 800°, and 1000°C. The amount of tetragonal phase is found to decrease with increase of temperature. The oxide texture of $(002)_m$ and $(11\bar{1})_m$ type increased with the temperature from 400°C to 600°C, however at temperatures above 600°C the texture strength seems to diminish and the oxide layer becomes structurally unstable. Further, the impedance response is found to be dependent on the microstructure of the oxide film. For the sample oxidized at 400°C, Electrochemical Impedance Spectroscopy (EIS) spectra exhibited a two-time constant behavior, showing the formation of two-layer oxide film on the Zr-2.5Nb alloy, which correspond to a porous outer oxide and a barrier inner oxide, respectively. In addition, the samples were oxidized at constant temperature of 600°C with varying oxidation time. The observation shows that the oxide is more protective in the early stage of oxide growth. However, further growth of oxide film has resulted in degeneration of its protective character.

1. Introduction

Zirconium oxide formed on the surface of the tube plays a vital role in controlling the rate of oxidation and the pickup of hydrogen and deuterium. The oxide film extends the life of the pressure tube by acting as a barrier to hydrogen ingress. Zirconium oxide has three crystal structures, monoclinic, cubic and tetragonal. Monoclinic phase is stable at room temperature and tetragonal phase exists at a temperature above 1470°K at a pressure of 0.1 MPa [1]. However, detailed investigation with transmission electron microscopy demonstrated the existence of tetragonal phase at the metal/oxide interface [2]. The stress in oxide is a function of the thickness of the adherent un-cracked oxide layer, which contains a high percent of tetragonal zirconium oxide phase. The thickness of the un-cracked oxide layer is reported to vary from 2 μm to 4 μm [3].

The purpose of the present study is to investigate the high temperature oxidation behavior of Zr-2.5Nb at different temperatures. This information would be useful for an overall understanding of the oxidation process, and could also conceivably be used as the starting point for more detailed analysis of oxide at loss-of-coolant-accident conditions [4].

2. Experimental

The present analysis is done on Zr-2.5Nb pressure tube, which was extruded at 820-850°C, 20-30% cold worked, and then stress relieved in steam for 24h at 400°C. Samples of dimension 20 X 18 X 1 mm were machined from the pressure tube. The surfaces of the samples were made flat by mechanical milling and further polished using SiC paper down to 800 grids, so that, surface stresses created by the mechanical milling can be removed.

Initially, samples were oxidized at four different temperatures i.e, 400, 600, 800 and 1000°C, separately in oxygen atmosphere for a constant period of 1440min (i.e. 24h) using Split Hinge Tube Furnace. Commercially pure (> 99%) oxygen was used for oxidation at a constant gas flow rate of 2-3 ml/s, which is slow enough to avoid any buoyancy effects, and fast enough to give measurable oxidation rates [5].

Later, electrochemical impedance measurements were done on the oxide surface, in order to measure the effect of tetragonal phase, cracks, and pores of the oxide on its corrosion resistance. Focus was mainly kept on the samples oxidized in oxygen atmosphere at 400°C and 600°C, as these two temperatures were extensively studied and are close to the oxidation conditions employed in the nuclear industry [6, 7, 8, 9]. Autolab-302 was used for impedance measurement, and the electrolyte used for present experiment is distilled water. A three electrode cell consists of working electrode (WE), counter electrode (CE) and reference electrode (RE) [10]. The reference electrode used in the present experiment was the standard calomel electrode having a potential of +241 mV with respect to the standard hydrogen electrode. The counter electrode was made of a platinum wire, and the working electrode is the sample. The electrochemical impedance spectroscopy (EIS) is performed over a frequency range of 10^4 Hz- 10^{-3} Hz at Open Circuit Potential (OCP), with AC amplitude of +/- 10 mV at a scan rate of 1 mV/sec.

3.0 Results

3.1 X-Ray diffraction analysis

X-ray diffraction technique with phase identification software was used for effective quantification of monoclinic and tetragonal phases. The volume ratio of monoclinic to tetragonal zirconia were evaluated using polymorph method by considering intensities of $(11\bar{1})_m$, $(111)_t$ and $(111)_m$ diffraction peaks [11], where the subscripts t, m, stands for tetragonal and monoclinic phase.

The volume ratio of tetragonal phase V_t is calculated using following equations

$$V_t = \frac{X_t}{C(1-X_t)+X_t} \quad (1)$$

Where $C= 1.381$ for $\text{CuK}\alpha$, and

$$X_t = \frac{I(111)_t}{I(111)_m+I(111)_m+I(111)_t} \quad (2)$$

The X-ray diffraction analysis of oxide films confirms the presence of both monoclinic and tetragonal phases, in which, the monoclinic takes the major portion at all temperatures. Figure-1 shows the XRD patterns of samples oxidized at 400°, 600°, 800° and 1000° C. The diffraction data of samples obtained using $\text{Cu-K}\alpha$ radiation is compared with as-received Zr-2.5Nb.

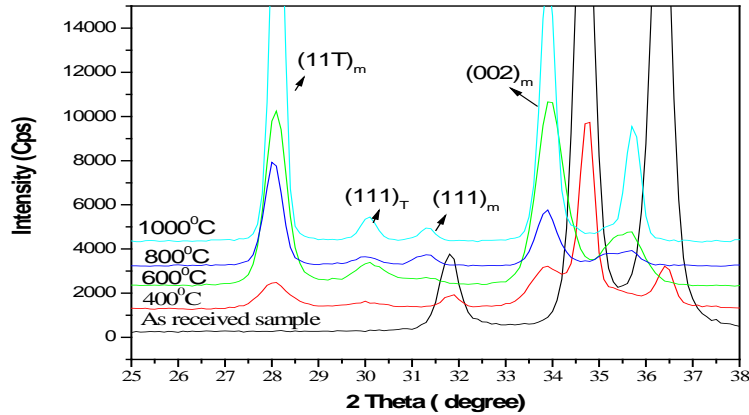


Figure-1: X-ray diffraction peaks of samples oxidized at different temperatures

The volume ratio of monoclinic to tetragonal zirconia was calculated by specific peak intensity using equation (2). It was found that the volume of tetragonal phase is decreasing with the increase in temperature from 400°C to 1000°C, irrespective of the mode by which sample were oxidized (see Figure-2). However, the decrease in tetragonal phase can be attributed to the oxide cracking, and the release of compressive stress, which is responsible for presence of tetragonal phase at room temperature.

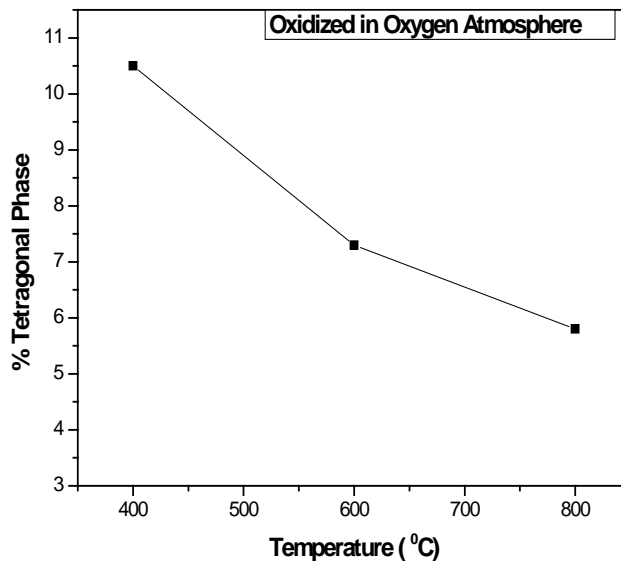


Figure-2: The variation of tetragonal phase in the oxide as a function of temperature

3.2 Thickness measurement

The thickness of the oxide is measured using scanning electron microscopy (SEM). The oxidized samples were cut along the rolling direction and all the four sides of the oxide layer are protected

with stainless steel, so that the damage of the oxide layer will be minimal during polishing. As expected, the SEM results showed the increase in thickness of the oxide with the increase in temperature (see Table-1).

Table-1: Thickness of oxide layer from 400 to 800°C

Thickness of the oxide layer (μm)	
Temperature in ($^{\circ}\text{C}$)	In Oxygen Atmosphere
	RD
400	0.72
600	15.85
800	522

*Note: RD = Radial direction of the pressure tube

3.3 Grain Size and Micro-strain

Grain size and micro-strain measurements were done using X-ray diffraction peak broadening. According to theory of kinematical scattering, the X-ray diffraction (XRD) peak is broadened due to small crystallite size, and strain caused by dislocations and stacking faults. The instrumental broadening can be eliminated by subtracting the broadening obtained by measurement of a standard ZrO_2 powder diffraction pattern. Profile fitting method is used to measure the broadening (FWHM – Full Width Half Maxima) of the strong peaks. Along with crystallite size, micro-strain data was simultaneously analyzed by solving the Williamson-Hall equation from the strong reflections [12].

Williamson-Hall Equation:

$$\beta \cos \theta = \left[\frac{K\lambda}{t} \right] + [4\epsilon \sin \theta] \quad (3)$$

Where t = crystallite size, K = Scherrer constant, λ = wavelength of radiation, ϵ = micro-strain and $\beta = \sqrt{((\beta_{\text{obs}})^2 - (\beta_{\text{std}})^2)}$ at an angle θ . Where β_{obs} is the observed FWHM value in radians and β_{std} is the FWHM value in radians of standard ZrO_2 powder.

The slope of the plot of equation (3) gives the micro-strain ϵ , and the interception with the vertical axis gives the crystallite size.

The micro-strain is found to decrease with the increase in temperature from 400°C to 800°C, whereas, the grain size is found to increase with the increase in temperature (see Figure-3). The obvious reason for decrease in micro-strain is oxide cracking that lowers the compressive stress at the oxide-metal interface.

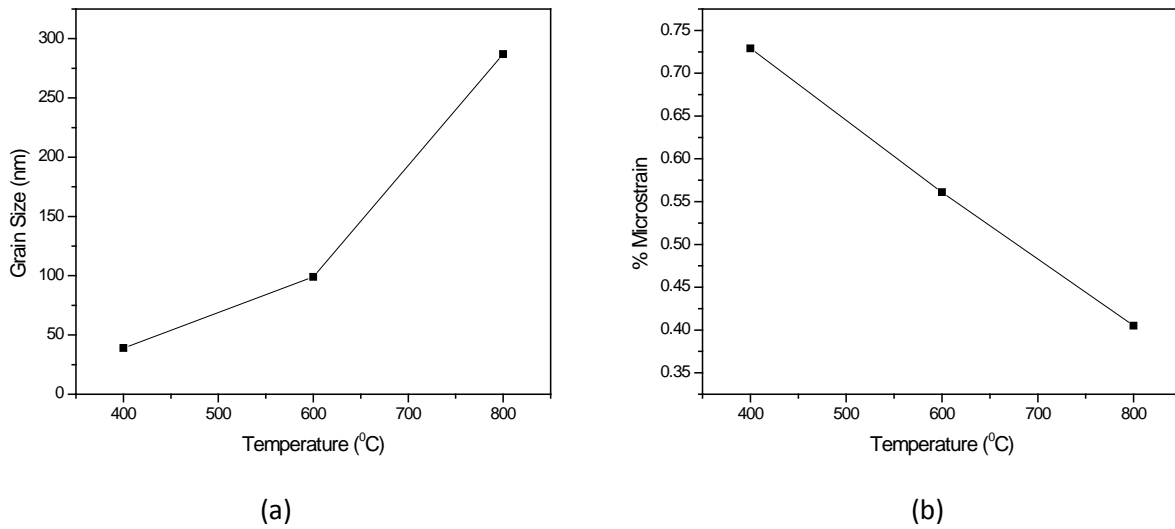


Figure-3: a) Grain Size and b) Micro-strain, of the oxide layer varying with temperature.

3.4 Oxide Morphology

Figures 4, shows the morphology of oxide grown on Zr-2.5Nb alloy at different temperatures. It can be clearly seen that the number of cracks are increasing with the increase in temperature. As discussed earlier, the oxide film formed on Zr-2.5Nb experience high compressive stresses, apart from that, with the increase in temperature, portion of untransformed tetragonal phase will also try to transform to monoclinic phase, which will indeed add to internal stresses around transformed zirconium grains. In addition, the change in oxidizing mechanism can be the other reason for increase in cracks density and change in morphology of oxide. Therefore, the combined compressive stresses have resulted in cracking of oxide layer.

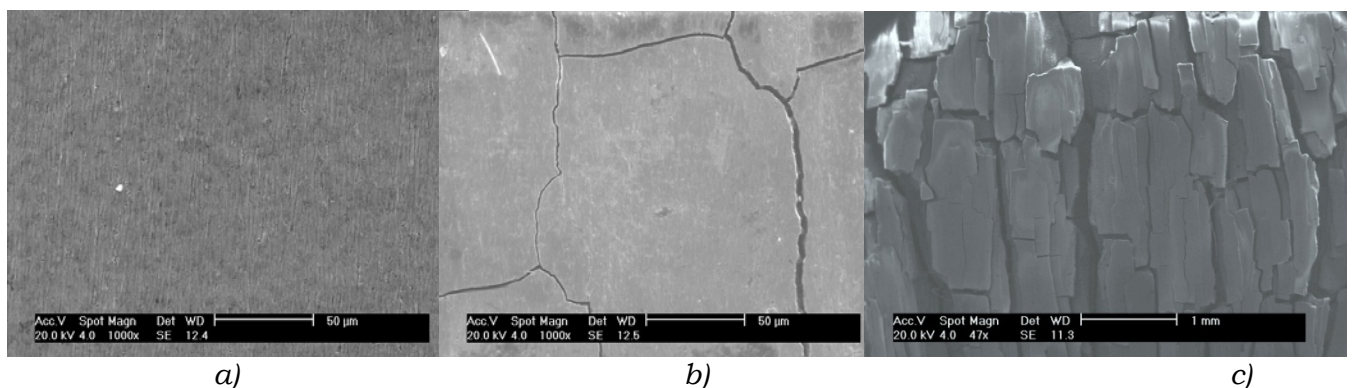


Figure-4: SEM images showing morphology of zirconium oxide formed on Zr-2.5Nb, at a) 400°C, b) 600°C, c) 800°C.

3.5 Texture

Texture measurements on oxidized samples were performed using X-ray diffraction technique. A texture free pure ZrO_2 powder was used in order to correct the experimental data. The $(11\bar{1})_m$, $(002)_m$ pole figures were measured on the oxide film. A significant increase in the sharpness of $(11\bar{1})_m$ texture is observed with the increase in oxidizing temperature from $400^\circ C$ to $600^\circ C$. This indicates that, there is an increase in the number of oxide grains, which grow with a well defined orientation (see Figures 5). On the other hand, a strong $(002)_m$ texture was observed in oxide. This is because of the influence of the underlying metal substrate, which has a strong (0002) texture. Therefore, the two-fold symmetry of (0002) underlying substrate manifests itself in the texture of the oxide by appearance of two-fold symmetry in the $(002)_m$ pole figure. However, the sharpness of $(002)_m$ texture is found to be decreasing with increase in temperature from 400° to 800° .

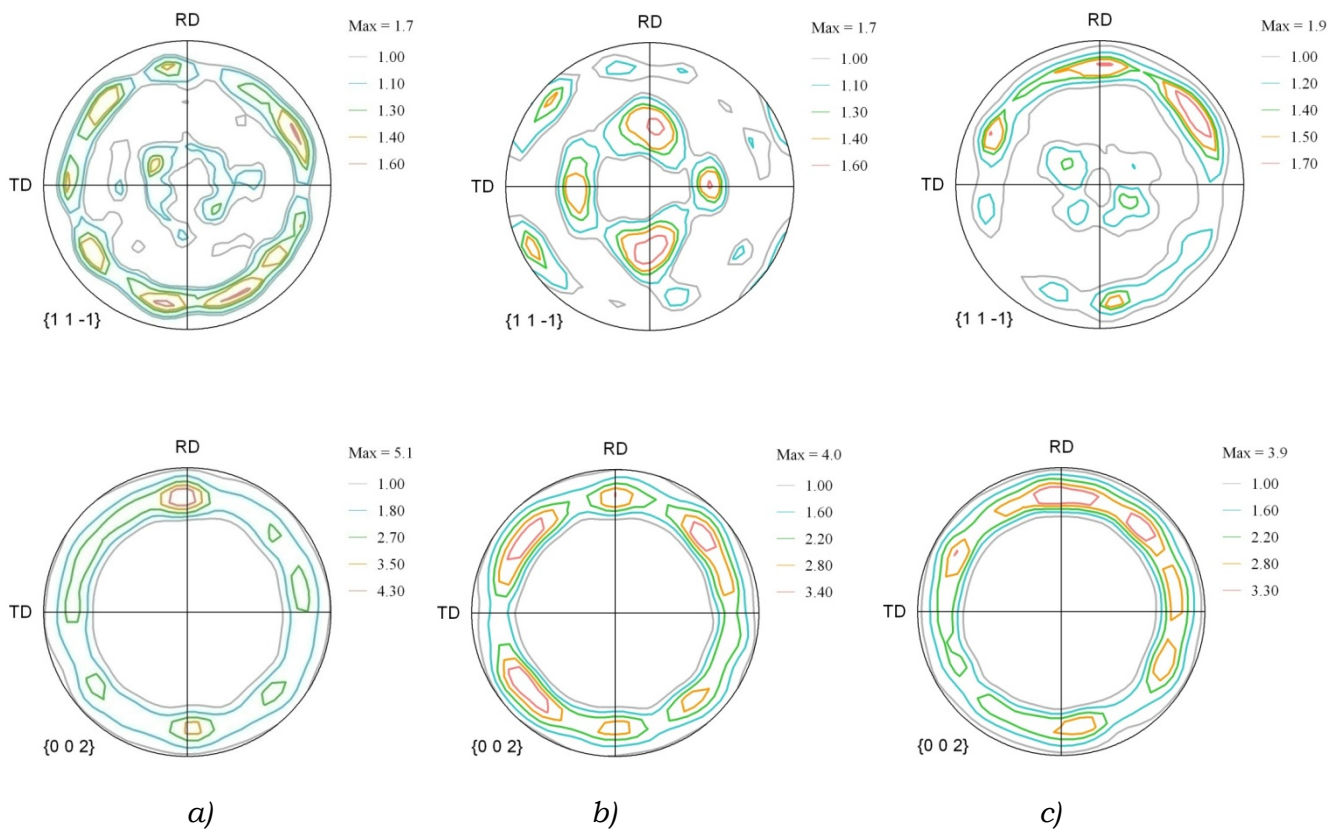


Figure-5: Comparison of $(11\bar{1})_m$ & $(002)_m$ pole figures of the monoclinic phase of zirconium oxide grown on Zr-2.5Nb at a) $400^\circ C$, b) $600^\circ C$ c) $800^\circ C$.

Urbanic et al. [13] have reported that the oxide grains formed in β -Zr region were typically of 5-15 nm in diameter, while the oxide grains formed over the α -Zr regions were much larger, 20-60 nm in diameter. So the oxide formed in β -Zr region contains high density of grain boundaries. As a result the rate of diffusion of oxygen through the oxide formed over the β -Zr regions is higher

than the oxide formed over the α -Zr regions. The amount of oxide grown by consuming α -Zr region, which have a well defined texture, increases with the increase of temperature from 400° to 600°C. However, at higher temperatures like 800°C, where the temperature is close to α - β transition temperature of 883°C, the fraction of β -Zr phase is higher, resulting in high oxidation rate and decrease in strength of texture.

3.6 Impedance Measurement

The impedance measurement was done on the samples oxidized at 400°C and 600°C, so that the effect oxide thickness and tetragonal phase on the corrosion resistance of the oxide can be analyzed. Initially the samples were immersed in distilled water for 1/2 hour to stabilize the open circuit potential.

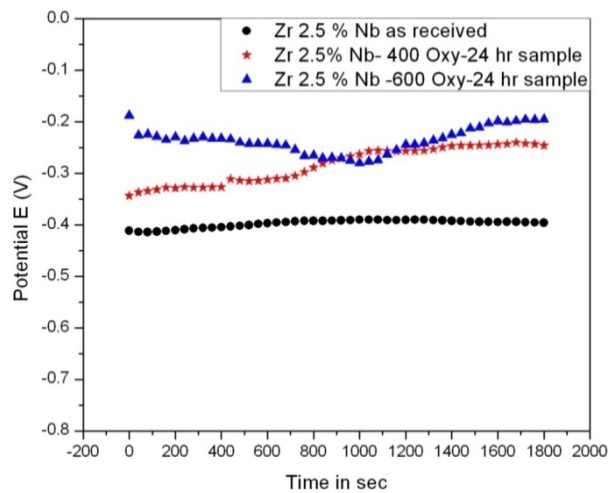


Figure-6: OCP of, i) As received, ii) 400°, iii) 600° samples

The open circuit potential of the samples oxidized at 400°C and 600°C for 24 hrs in oxygen atmosphere are compared with as received Zr-2.5Nb sample as shown in Figure-6. It was found that the resistance to charge transfer of the oxide is increasing with the increase in oxidation temperature. This can be due to the increase in thickness of the oxide with oxidation temperature, which will act as a barrier to charge transfer.

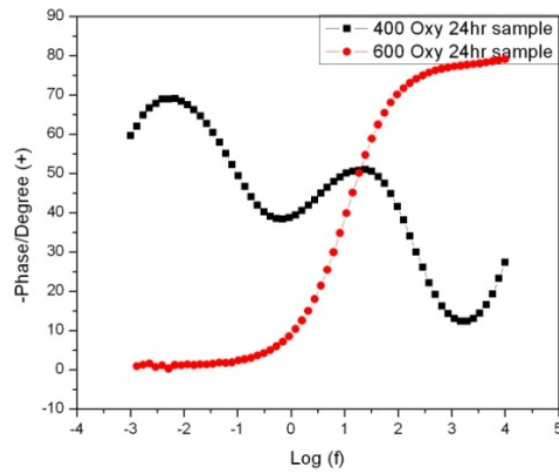


Figure-7: Bode plot (Phase angle vs Log (Frequency)) of samples oxidized at 400°C and 600°C for 24h

Once the OCP is stabilized, the impedance measurements were done on samples. The Bode plot of samples oxidized for 24 hrs at 400°C and 600°C is shown in Figure-7. The spectra of 600°C oxide sample exhibits one-time constant behavior, since only one peak is observed on the phase vs frequency curve, whereas 400°C sample exhibits two-time constant behavior with two peaks. Many electrical circuits were proposed in the literature to model EIS spectra of oxide layer. The most commonly used equivalent circuits for one peak and two peak oxides are shown in Figure-8.

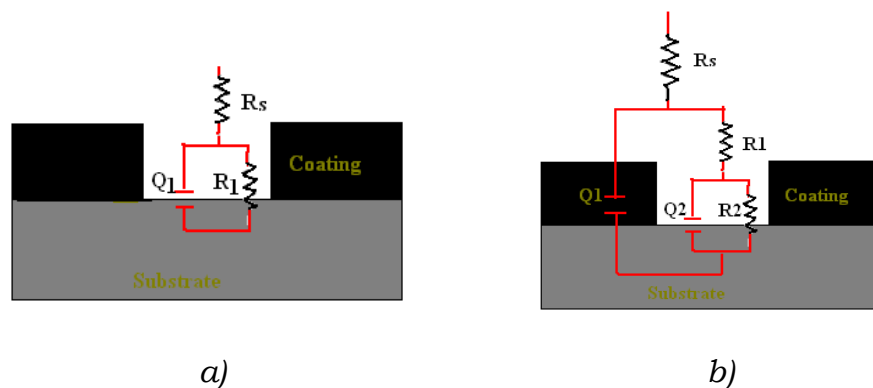


Figure-8: Equivalent electrical circuit for modeling EIS spectra of a) 600°C, b) 400°C Oxides.

The phase elements Q_1 and Q_2 in these electrical circuits represent the charge or discharge that occurs at the film/electrolyte and substrate/electrolyte. The substrate/electrolyte charge or discharge is due to infiltration of the electrolyte through the film pores to reach the substrate.

It was observed that with increase in oxidation temperature from 400°C to 600°C, the electric circuit of the oxide has changed from complex R_s (Q_1 [R_1 ($Q_2 R_2$)]), as shown in Figure-8(b), to

a simple Rs (R_1Q_1) circuit Figure-8(a). This behavior of the oxide layers formed at 400°C and 600°C can be due to two factors

- i) Increase in oxide thickness.
- ii) Change in concentration of tetragonal phase in the multi phased oxide layer.

In-order to understand the change in corrosion resistance of the oxide layers, series of samples were prepared by varying oxidation time at constant temperature of 600°C. All the samples were oxidized in autoclave at 600°C in the flow of oxygen at 2 -3 ml/s. The oxidation time used were 1) 0.5 h, 2) 1h, 3) 2 h, 4) 4h, 5) 8h, 6) 16 h and 7) 24h. The thickness of the oxide layer is shown in the Figure-9.

Interestingly, the volume of tetragonal phase is found to be decreasing with the increase of in oxidation time (see Figure-10). This can be attributed to the increase in number of cracks and decrease of the residual stress, which are responsible for the presence of unstable tetragonal phase at room temperature.

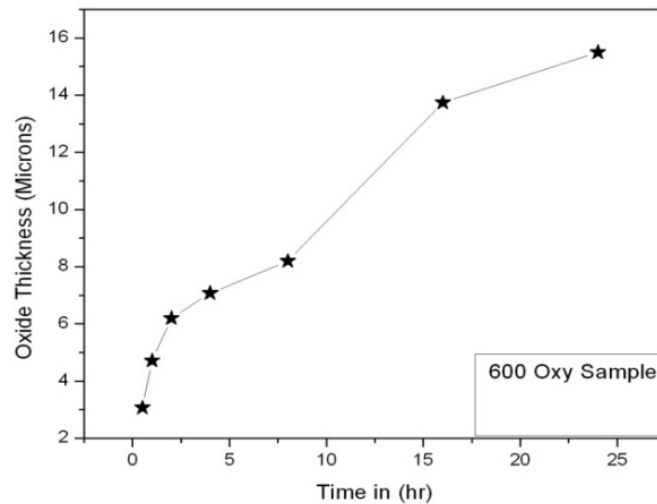


Figure-9: Oxidation Time vs Thickness plot of samples oxidized at 600°C

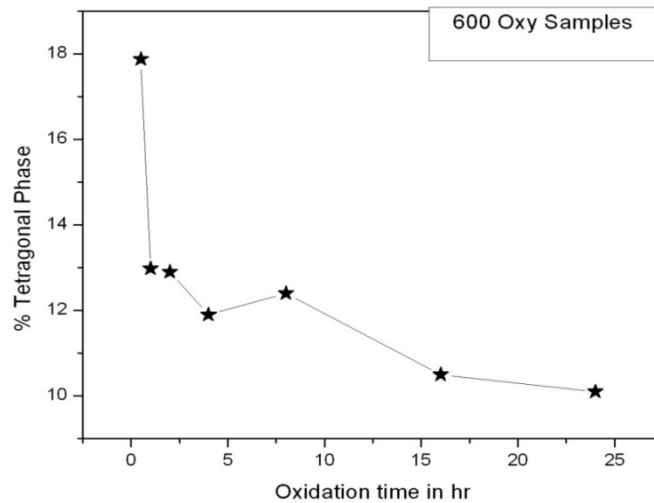


Figure 10: The effect of oxidation time on percentage of tetragonal phase

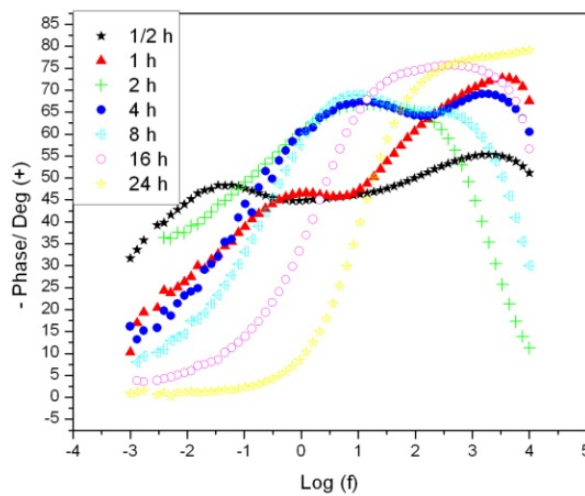


Figure-11: Bode diagram of samples oxidized at 600°C with oxidation time varying from 0.5 to 24 hrs

The Bode diagram of the samples oxidized at 600°C at varied time is found to be changing with change in oxidation time (see Figure 11). The spectrum has one time-constant on 24h sample, and it changes into two time-constant with decrease in time of oxidation. The change from two time-constant to one time-constant with increase in the oxide thickness can be due to the increase in pore size which becomes large and it makes the resistance to infiltration R1 very low. As a result the circuit becomes simpler. Since the thickness difference between 400°C-24h oxidized sample and 600°C-½ h oxidized samples is small (1-2 μm) the impedance data of these two samples can be compared. Figure-12 shows the Bode diagram of 400°C-24h and 600°C- ½ h oxidized samples.

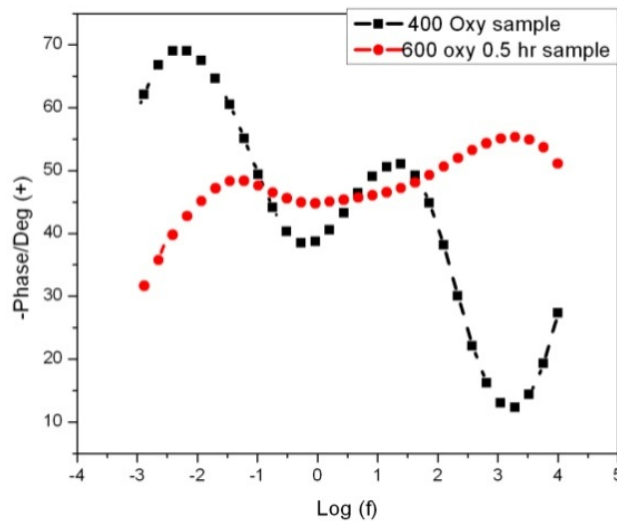


Figure-12: Bode diagram of 400°C-24h and 600°C - ½ h samples

A complex $R_s (Q_1 [R_1 (Q_2R_2)])$ circuit is used to model the impedance data. The data obtained from the modeling are presented in Table-2.

Table-2: The data obtained from the EIS spectra simulation

Sample	R_s ($k\Omega \cdot cm^2$)	$Q_1(Y_0)$ (F/cm^2)	Q_1 (n)	R_1 ($M\Omega \cdot cm^2$)	$Q_2 (Y_0)$ (F)	Q_2 (n)	R_2 ($M\Omega \cdot cm^2$)
400°C-24h	0.4	0.27×10^{-6}	0.62	0.568	0.35×10^{-6}	0.62	45
600°C-½h	1.89	0.28×10^{-6}	0.72	0.863	1.11×10^{-6}	0.85	233.5

Since the polarization resistance of the oxide (see Table-2) was changing with the tetragonal phase, it is evident that the tetragonal phase is playing important role in controlling corrosion behavior of zirconium alloy oxides.

For 400°C-24h oxidized sample, the polarization resistance R_2 , is $45 \text{ MOhms} \cdot cm^2$ compared to $233.5 \text{ MOhms} \cdot cm^2$ for the 600°C- ½ h sample indicating that the 600°C-0.5h sample with high tetragonal phase is showing better corrosion resistance than 400°C-24h sample. The high value of ionic resistance to pores R_1 observed in 600°C-0.5h sample indicates that 400°C-24 h sample is less resistant against infiltration of electrolyte through the film to reach the substrate.

4.0 Summary

The amount of tetragonal phase is found to be decreasing with increase in temperature. This phenomenon is related to decrease of micro stress and increase of thickness of the oxide layer. The oxide layer becomes structurally unstable in high temperatures ($\geq 600^{\circ}\text{C}$), based on SEM observations. The results of the SEM observation are consistent with EIS studies. EIS test is a non-destructive process that provides important information in monitoring the evolution of microstructure of ZrO_2 film. The strength of (111) oxide texture increases with increasing temperature from 400°C to 600°C . The two-fold symmetry of (0002) underlying substrate manifests itself in the texture of the oxide by appearance of two-fold symmetry in the (002) pole figure.

The electrochemical impedance response is dependent on the microstructure of the oxide film. For the sample oxidized at 400°C , EIS spectra exhibited a two-time constant behavior, showing the formation of two-layer oxide film on the Zr-2.5Nb alloy, which correspond to a porous outer oxide and a barrier inner oxide, respectively. A bi-layered structure of the oxide film may therefore be confirmed using EIS technique. The electrochemical impedance response was simulated with an equivalent electrical circuit to determine the resistances and the capacitances in dense barrier layer and pore layer, respectively.

For the sample oxidized at 600°C , the observation of EIS spectra found that at initial stage of oxidization, EIS spectra exhibited a two-time constant behavior, but gradually transition to the one-time constant behavior was observed with increasing time (> 16 hours). The total impedance amplitude $|Z|$ is the highest in the initial stage of oxidation, but decreases when the oxidation time is longer than 16 hours. These results indicate that the oxide is protective in the early growth stage, which is also associated with the increase in the thickness of oxide film. However, as indicated by EIS spectra, further growth of ZrO_2 film will result in the deterioration of the protective character of oxide. Such a change is attributed to an increase of number of cracks in the outside layer of the oxide film and the interconnecting of them. The electrolyte can pass through such cracked region and reach the underlying dense layer, which results in the transformation from the two-time to the one-time constant behavior, and simultaneously total impedance amplitude $|Z|$ decreases. By the observation of change in EIS spectra, we may non-destructively and in real-time monitor the formation and the growth of cracks and porosity in the oxide film formed on the Zr-2.5Nb tubes.

5.0 Conclusions

The high temperature oxidation of Zr-2.5Nb alloys is investigated by varying oxidization temperature from 400°C to 1000°C . The analysis of EIS spectra was done on the samples oxidized in autoclave at different temperatures. Impedances measurements were carried out over a frequency range of 10^{-3} Hz- 10^4 Hz. The electrolyte used in the present experiment was distilled water.

1. XRD measurements show that the percent of tetragonal phase substantially decreases with increasing oxidation time. This implies that there is the transformation from the tetragonal phase to the monoclinic phase. The internal stress induced by such a phase

transformation is a fundamental reason for the formation of pores (cracks) in the outside layer of ZrO₂ film.

2. The two-fold symmetry of the (002)m oxide is generated by a strong two-fold symmetry of (0002) planes in the substrate.
3. The impedance, resistance to charge transfer, and the capacitance are found to be a function of the thickness and the density of oxide. Based on the observation of impedance spectra, we may non-destructively analyze the evolution of porous outer layer and a barrier inner layer in the corrosion processes.
4. The oxidation resistance is higher in the early growth stages of oxidation. However, the protective character of oxide decreases for thicker oxides due to large number of cracks.

References

- 1) A.E.Mchale, R.S. Roth, Phase equilibrium Diagrams, The American Ceramic Society, Vol. XII, Ohio, (1996), 8-10.
- 2) Y.P.Lin, O.T.Woo, D.J. Lockwood, Texture and Phases in Oxide. Films on Zr–Nb Alloys, Mat. Res. Soc. Symposium. Proc, 343, (1994), 487- 492.
- 3) A.M.Garde, G.P. Smith, and R.C. Pirek, Effects of Hydride Precipitate Localization and Neutron Fluence on the Ductility of Irradiated Zr-4, 11th Inter. Symposium, PA: ASTM, (1996), 407-430.
- 4) A.J.White, A.Sawatzky, S.Jones, G.A.Ledoux, A failure criterion for CANDU fuel cladding subjected to thermal-quench loads, American Nuclear society, (1991), 555-562.
- 5) R. Kohli, High temperature oxidation of some zirconium alloys in flowing oxygen Journal of Nuclear materials, 91, (1980), 85-92.
- 6) P. Barberis, T. Merle-Méjean and P. Quintard, On Raman spectroscopy of zirconium oxide films, Journal of Nuclear materials, 246, (1997), 232-243.
- 7) H. Blank, G. Bart, H. Thiele, Structural analysis of oxide scales grown on zirconium alloys in autoclaves and in a PWR, Journal of Nuclear Materials, 188, (1992), 273-279.
- 8) J. Lin H. Li, J.A. Szpunar, R. Bordoni, A.M. Olmedo, M.Villegas, A.J.G. Maroto, Analysis of zirconium oxide formed during oxidation at 623 K on Zr–2.5Nb and Zircaloy-4, Materials Science and Engineering A, 381, (2004), 104–112.
- 9) M.G. Glavicic, J.A. Szpunar, Y.P. Lin, A method for the quantitative phase analysis of ZrO₂ films grown on Zr-2.5% Nb pressure tubes, Journal of Nuclear Materials, 245, (1997), 147-151.
- 10) H. Göhr, J. Schaller, C.A. Schiller, Impedance studies of the oxide layer on zircaloy after previous oxidation in water vapour at 400°C. Electrochimica Acta, 38, (1993), 1961-1964.
- 11) J.Li, X. Bai and D. Zhang, Characterization and structure of the anodic oxide film on Zircaloy-4 synthesized using NaOH electrolytes at room temperature, Applied surface science, 252, (2006), 7436-7441.
- 12) E. Koray Akdogan and Ahmad Safari, Crystallite size and microstrain studies in high purity submicron barium titanate powders, Proceedings of the Tenth IEEE International Symposium, 2, (1996), 1007 – 1010.
- 13) V.F. Urbanic, T.R. Heidrick, High-temperature oxidation of zircaloy-2 and zircaloy-4 in steam, Journal of Nuclear Materials, 75, (1978), 251-261.